IEEE Photonics Journal
An IEEE Photonics Society Publication

Open Access

Far-Field Super-Resolution Imaging of Scatterers With a Time-Reversal System Aided by a Grating Plate

Volume 9, Number 1, February 2017

Zhi-Shuang Gong
Bing-Zhong Wang, *Senior Member, IEEE*
Yu Yang
Hong-Cheng Zhou
Shuai Ding
Xiao-Hua Wang, *Member, IEEE*

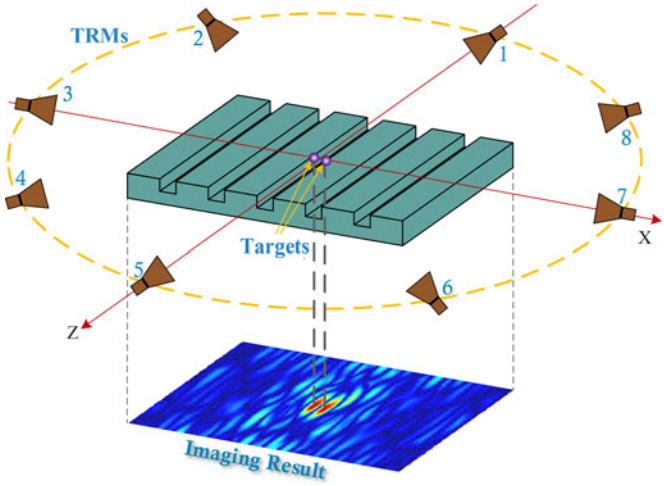

DOI: 10.1109/JPHOT.2016.2640661
1943-0655 © 2016 IEEE

IEEE photonics SOCIETY

IEEE

Far-Field Super-Resolution Imaging of Scatterers With a Time-Reversal System Aided by a Grating Plate

Zhi-Shuang Gong, Bing-Zhong Wang, *Senior Member, IEEE*, Yu Yang, Hong-Cheng Zhou, Shuai Ding, and Xiao-Hua Wang, *Member, IEEE*

Institute of Applied Physics, University of Electronic Science and Technology of China, Chengdu 610054, China

DOI:10.1109/JPHOT.2016.2640661

Manuscript received October 17, 2016; revised December 4, 2016; accepted December 11, 2016. Date of publication December 15, 2016; date of current version January 5, 2017. This work was supported by the National Science Foundation of China under Grant 61331007, Grant 61301271, Grant 61571085 and Grant 61361166008, and by the Open Fund of State Key Laboratory of Satellite Ocean Environment Dynamics, Second Institute of Oceanography (SOED1507). Corresponding author: Z.-S. Gong (e-mail: centuryhh@gmail.com).

Abstract: A time-reversal imaging system for far-field super-resolution imaging of scatterers is proposed. First, a grating plate, similar to the optical far-field super lens, is designed to convert near-field evanescent waves to propagative waves with wavevector modulation. Then, the scattered signals are processed by a time-reversal (TR) technique and retransmitted back. Finally, the images of the targets are reconstructed by doing demodulation operations in the *k*-domain to the TR field at the refocusing time. Imaging results show that two scatterers separated by 0.1 λ can be distinguished clearly.

Index Terms: Super-resolution imaging, far-field, time reversal (TR).

1. Introduction

Resolution of theof conventional imaging lens is generally constrained by the diffraction limit, which prevents the imaging of subwavelength features. Such fine details are encoded in rapid spatial variations of electromagnetic fields over the surface of the object. However, these fields suffer exponential decay with distance and thus only being detectable in the near field. Outside of the near field, the loss of high spatial frequency information carried by the decaying evanescent waves precludes reconstructing the image of an object with resolution better than the diffraction limit.

Subwavelength imaging can be performed with help of a slab of left-handed material for the enhancement of evanescent waves in the slab [1]. However, the realization of left-handed material encounters multifarious challenges. Alternatively, super-lens has been proposed to enhance evanescent waves with help of thin metal plates since metals have negative permittivity at optical frequencies [2]. However, these methods are only suitable for near-field applications due to the decay outside of the lens. In order to realize far-field subwavelength imaging, Zhang proposed the far-field super-lens at optical wavelengths [3]–[5]. Owing to the plate with corrugated surfaces, a portion of evanescent waves could be converted to propagative waves and thus be transmitted to far-field. During the imaging phase, charged-coupled device (CCD) cameras are used to collect the field distribution information.

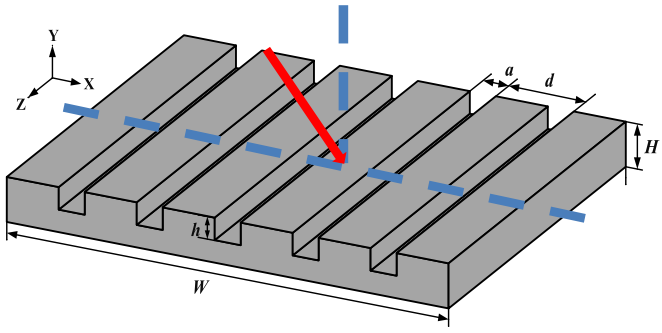

Fig. 1. Structure of the grating plate.

Speaking of microwave imaging applications, similar devices such as hyper-lens have also been proposed with their functions been proved in [6] and [7]. This kind of lens can indeed convert evanescent waves to propagative waves. However, there is no imaging method which has been proposed to reconstruct the image of scatterers with the lens. And since the wavelength of microwave is much larger than that of optical wave, the size of microwave camera will be very large. Therefore, the method of using microwave camera, which is similar with the method being used in optical region, to collect field distribution information in far-field region at microwave wavelengths will not be a good solution.

Time-reversal (TR) technology has been studied quite intensively at recent years for its attracting property of refocusing fields to the original source point. One of the most astonishing results obtained using TR of electromagnetic waves is that the diffraction limit can be surpassed with microstructured materials, or in other words, that the electromagnetic waves can be focused on deep subwavelength spots in the far-field region [8], [9]. This property makes TR an excellent alternative for image reconstruction procedures.

In this paper, we proposed a TR imaging system aided by a grating plate with the function of converting near-field evanescent waves to propagative waves. During Section II, the working mechanism of our designed system is introduced theoretically. And then, the TR image reconstruction method is described detailedly. In Section III, an imaging experiment is performed to show the effect of our proposed imaging system. The imaging result shows that our system can provide an imaging resolution far below the diffraction limit.

2. Principle of the Imaging System

Super-resolution images of targets can be formed only when both propagative and evanescent informations are exploited. Different from propagative signals, evanescent signals cannot be received naturally in far-field region. For the purpose of realizing far-field super-resolution imaging at microwave frequencies, a grating plate is designed, similar with the fabrication of the optical super-lens [4]. As shown in Fig. 1, the structure is composed of a metal ground and a finite number of metal gratings with a period of d. The width of each grating in the x-direction is d-a in a rectangular coordinate system. All the gratings have a same height of h, and the height of the ground is H-h.

2.1. Evanescent-to-Propagating Conversion

For a transverse magnetic (TM) polarized plane wave incidents onto the surface of the grating plate as shown in Fig. 1 with wavevector $\boldsymbol{k}_0$. According to the Floquet theory and the mode expansion approach [10], the total field $\boldsymbol{u}(\boldsymbol{r})$ ($\boldsymbol{u}$ stands for the magnetic field H for TM polarized wave) in the upper space, which is the summation of incident wave $\boldsymbol{u}^{inc}$ and reflection wave $\boldsymbol{u}^{ref}$, can be

expressed as

$$\boldsymbol{u}(\boldsymbol{r}) = \boldsymbol{u}^{inc}(\boldsymbol{r}) + \boldsymbol{u}^{ref}(\boldsymbol{r}) = \left(e^{j\boldsymbol{k}^{inc}\cdot\boldsymbol{r}} + \sum_{n=-\infty}^{+\infty} B_n e^{j\boldsymbol{k}_n^{ref}\cdot\boldsymbol{r}} \right) \boldsymbol{e}_z$$
$$= \left(e^{ik_x x - ik_y y} + \sum_{n=-\infty}^{+\infty} B_n e^{j(nk_d + k_x)x + i\beta_n(y-h)} \right) \boldsymbol{e}_z \tag{1}$$

where $k_d = 2\pi/d$ is the grating wavenumber. k_x and k_y are the amplitudes of the x and y components of the incident wavevector, respectively. $\boldsymbol{e}_z$ is the unit vector in the z-direction. $\beta_n = \sqrt{k_0^2 - (k_x + nk_d)^2}$ is the vertical wavevector of the nth-order diffraction wave. In other words, the grating plate can provide modulation of the incident wave in the transverse wavenumber, by integer increments of k_d. Once a plane wave incidents onto the surface, the reflection wave would have many diffraction orders with their transverse wavevector of $\tau_n = k_x + nk_d$, whose amplitudes are B_n. Obviously, a portion of incident evanescent waves whose transverse wavenumbers locate in the region $(-k_0 - nk_d, k_0 - nk_d)$ will be transferred to propagative waves. Now, let us calculate the coefficients B_n [11].

For the groove region, the system can be regarded as a parallel-plate system with one side shorted. Therefore, the total field can be expressed as:

$$\boldsymbol{u}(\boldsymbol{r}) = \left(\sum_{m=0}^{+\infty} a_m \cos(\mu_m y) \cos\left(\frac{m\pi x}{c}\right) \right) \boldsymbol{e}_z \tag{2}$$

where $\mu_m = \sqrt{k_0^2 - (m\pi/c)^2}$ is the propagation constant of the m-th parallel-plate mode. Applying the boundary conditions on the interface between the upper space and the groove region, the relationship between the coefficients B_n and a_m can be finally obtained as

$$\sum_{m=0}^{+\infty} \frac{-\mu_m}{d} a_m \sin(\mu_m h) S_{nm} = i\beta_n B_n - ik_y \delta_{n0} e^{-ik_y h} \tag{3}$$

$$\sum_{m=0}^{+\infty} \frac{1}{d} a_m \cos(\mu_m h) S_{nm} = \sum_{m=-\infty}^{+\infty} c_{n-m} \left(B_m + \delta_{m0} e^{-ik_y h} \right) \tag{4}$$

where

$$c_n = \begin{cases} \frac{1}{2n\pi i}\left[1 - e^{-ink_d c}\right], & n \neq 0 \\ \frac{c}{d}, & n = 0 \end{cases} \tag{5}$$

$$S_{nm} = \int_0^c \cos\left(\frac{m\pi x}{c}\right) e^{-i\tau_n x} dx$$
$$= \begin{cases} \frac{i\tau_n c^2}{m^2\pi^2 - \tau_n^2 c^2}\left[1 - (-1)^m e^{-i\tau_n c}\right], & m\pi \neq \tau_n c \\ \frac{c}{2}, & m\pi = \tau_n c. \end{cases} \tag{6}$$

For a specific structure, solving the linear equations (3) and (4), the coefficients B_n can be obtained easily by numerical method. The corresponding results of our designed structure will be shown in the following part.

In order to reconstruct an unambiguous image of the target, there should be a one-to-one relationship between near-field information and far-field signature. It requires that the reflection coefficient of the main diffraction order should be much larger than the others, so that the other orders can be neglected [4]. The values of all the parameters in our designed grating are shown in Table 1. Fig. 2 shows the corresponding reflection coefficient of the order which make the waves to be converted to propagative waves at 6 GHz. It can be seen clearly that the reflection coefficient of $+1$st order is much larger than the -1st order. Therefore, in this case, we can suppose that the

TABLE 1
The Values of the Basic Parameters in the Structure

Name of parameter	Value	Name of parameter	Value
a (mm)	6	*W* (mm)	96
d (mm)	16	*h* (mm)	10

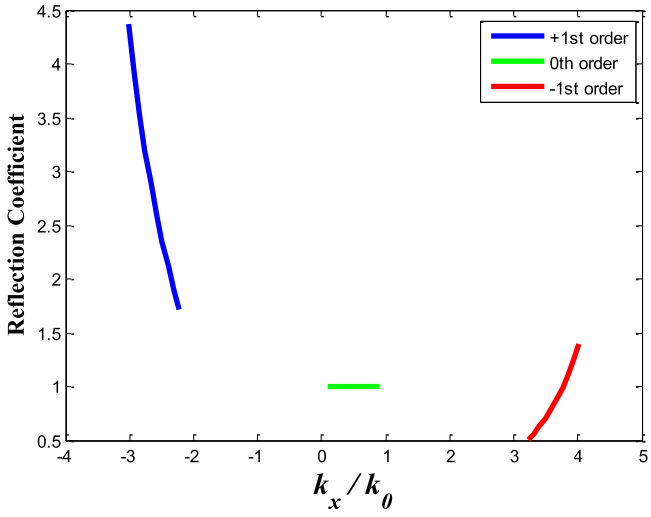

Fig. 2. Reflection coefficients with different incident waves for the order which make them to be converted to propagative waves at 6 GHz.

far-field transferred propagative modes only come from the +1st-order diffraction. Note that the higher orders are neglected since their amplitudes are usually much smaller than the ±1st orders [5].

2.2. Time-Reversal Imaging

With the evanescent informations having been recorded in far-field region, TR technology can be used to reconstruct the image of targets. In a conventional TR experiment, some sequential steps are required. First, during the forward phase, a pulse must be sent from a source placed in the desired focalization location. Then the radiated signals are collected by a set of receptors, which are usually called time-reversal mirrors (TRMs). Finally, during the TR phase, the recorded signals are reversed in time and reemitted by the same TRMs. By these steps, the wave would converge to the initial source. In the case of imaging, the targets can be regarded as secondary sources and the time reversal waves will converge to the position of targets. According to this property, the images of targets can be reconstructed by recording the refocusing positions of time reversal field.

The schematic view of the imaging system is shown in Fig. 3. The center working frequency of the system is 6 GHz. Two metal spheres are placed in the near-field of the grating plate as targets. These two targets, each with a radius of 1 mm, separated by 5 mm in the *x*-direction, are located at a plane 2 mm above the grating plate. More specifically, in the rectangular coordinate system shown in Fig 3, the positions of the two targets are (2.5 mm, 0, 0) and (−2.5 mm, 0, 0). Antennas 1–8 are placed uniformly around the grating plate in the circle with a radius of 3 m in the plane of $y = 0$, and the position of Antenna 1 is (0, 0, −3 m).

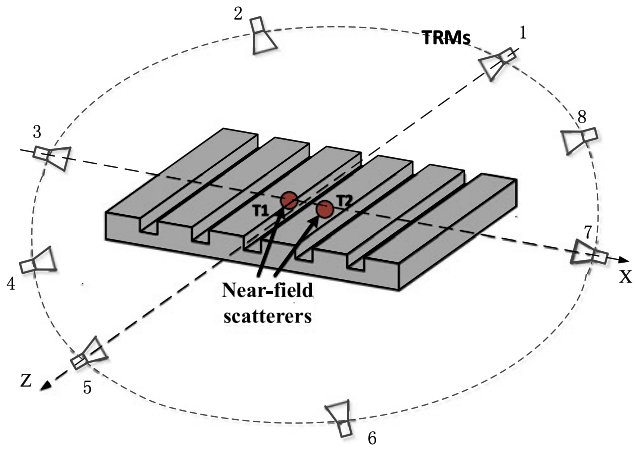

Fig. 3. Schematic view of the experimental system.

With these configurations, Antenna 1 is set as the source antenna and emits a signal. The incident electromagnetic wave illuminates the targets. Next, part of the fields scattered by targets will incident on the grating and then be modulated. At this step, some part of evanescent waves will be transferred to propagative waves. Actually, there exist four parts of propagative waves: the one propagating from the transmitting antenna to the receiving antennas (Part 1); the one scattering by the targets (Part 2); the one being transferred from the scattered evanescent waves of targets (Part 3), which only comes from the $+1$ diffraction order according to the analysis above; and the one scattering by the grating plate (Part 4). In the far-field region, all the four parts are mixed together. In order to reconstruct the scattering fields of targets, only Parts 2 and 3 are needed. These two parts can be extracted out by the following steps.

1) Record the received signals by the N TRMs as P_{0i} $(i = 1 \ldots N)$ when both the targets and the grating are taken away. In our case, $N = 8$.
2) Record the received signals by the N TRMs as P_{1i} $(i = 1 \ldots N)$ when only the targets exist.
3) Record the received signals by the N TRMs as P_{2i} $(i = 1 \ldots N)$ when only the grating plate exists.
4) Record the received signals by the N TRMs as P_{3i} $(i = 1 \ldots N)$ when both the grating plate and the targets exist.

Then, the propagative signals of Part 2, S^i_{pro}, can be achieved by subtracting P_{0i} from P_{1i}. The propagative signals of Part 3, S^i_{eva}, can be got as follow: $S^i_{eva} = P_{3i} - (P_{2i} - P_{0i}) - (P_{1i} - P_{0i}) - P_{0i} = P_{3i} - P_{2i} - P_{1i} + P_{0i}$, which are transferred from the scattered evanescent waves of targets.

Flipping S^i_{pro} and S^i_{eva} back in time and retransmitting them out by the same receivers, separately. The TR field getting from S^i_{pro} corresponds to the scattering propagative field of the targets. For the TR field getting from S^i_{eva}, it originates from the scattering evanescent field but has been modulated by the grating. The original scattering evanescent field can be got by kicking away the modulating component nkd. This can be realized by the following steps.

1) Record the TR field getting from S^i_{eva} as F_{eva}, and then, the corresponding spatial spectrum distribution A^{Mod}_{eva} can be calculated through spatial Fourier transform.
2) Find out the main diffraction order n, which is $+1$ in this case. The original spectrum distribution of the scattered evanescent wave (A_{eva}) can be had by translating A^{Mod}_{eva} with $-k_d$.
3) Do the inverse Fourier transform to A_{eva}, and then, the scattering evanescent field distribution of the targets can be achieved.

The spatial spectrum distribution of the scattering propagative mode (A_{pro}) can be achieved by doing spatial Fourier transform to the TR field getting from S^i_{pro}. Finally, the images of targets can be had by doing inverse spatial Fourier transform to $A_{pro} + A_{eva}$.

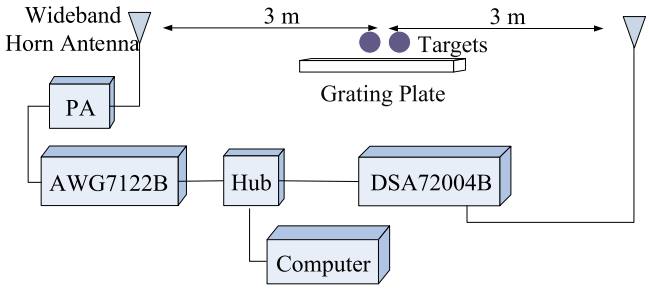

Fig. 4. Diagram of the experimental system.

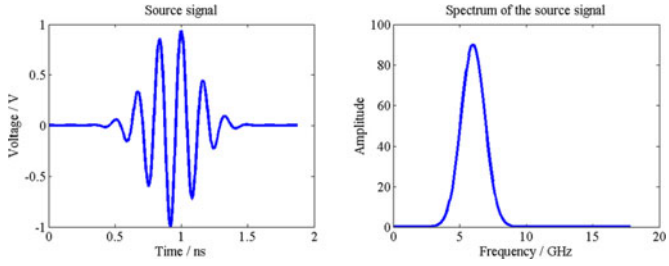

Fig. 5. The Waveform and spectrum of the excitation signal.

3. Imaging Results

To validate the effect of our method, an imaging experiment is performed. Fig. 4 gives the diagram of the experiment. According to the steps in Section II-B, the excitation signal transmitted by Antenna 1 (wideband horn antenna with working frequency band of 2–8 GHz) is a modulated Gaussian pulse with frequency spectrum from 4.1 to 7.9 GHz. The waveform and corresponding spectrum of the excitation signal are shown in Fig. 5. Then all the scattering signals in different cases are recorded by the TRMs (the same antennas as Antenna 1). Therefore, in the phase of imaging, a MATLAB program is coded to process these signals, extract the field distributions, and form the last imaging result.

Fig. 6(a) and (b) shows the TR field at the time when the TR field is focused at Target 1 and its corresponding spatial spectrum distribution (A_{pro}) when S^i_{pro} ($i = 1 \ldots 8$) were retransmitted by TRMs. Fig. 6(c) and (d) are the corresponding results when S^i_{eva} were retransmitted. It can be seen from Fig. 6(d) that the modulated evanescent components mainly contain two parts, as being labeled in the figure, the $+$1st-order part and $-$1st-order part. It has been proved by Fig. 2 that the far-field transferred propagative modes mainly come from the $+$1st-order diffraction. By neglecting higher order diffractions except the $\pm$1st orders, the demodulating operation can be realized by translating the $-$1st-order by $-k_d$. Similarly, for the $+$1st-order, the demodulation can be done by translating it by $+k_d$. Schematic of the demodulation is shown in Fig. 7(a). After demodulation, the resulting spectrum is just A_{eva}. Make combination of A_{pro} and A_{eva}, we will get the spectrum of the scattering field of Target 1, as shown in Fig. 7(b). By doing inverse spatial Fourier transform to Fig. 7(b), the image of Target 1 can be achieved as shown in Fig. 7(c). Similarly, the image of Target 2 can be had, as shown in Fig. 7(d).

Until now, the images being obtained only contain evanescent informations of targets in the *x*-direction since the *x*-orientated grating can only provide spatial spectrum modulation in the *x*-direction. By rotating the grating several degrees around the *y*-axis at one time, and with the similar steps, we can get the images of the targets with evanescent informations in several other directions being collected. Therefore, the images of the targets can be got at last by combining all the images together. Fig. 8 contains the images of the two targets with evanescent informations in 0, 45, and 90 degrees combined. Obviously, the spot sizes of the images are decreased remark-

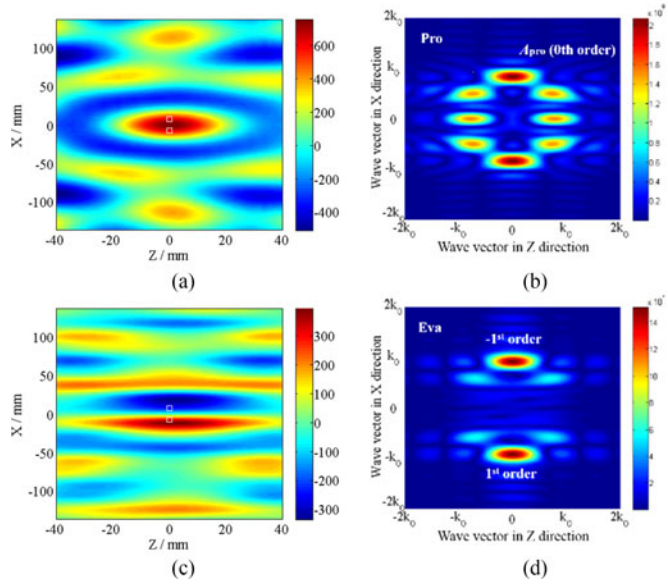

Fig. 6. Refocusing TR field and the corresponding spatial spectrum. k_0 is the wavenumber in vacuum at 6 GHz. In (a) and (b), only propagative signals were retransmitted; in (c) and (d), only evanescent signals were retransmitted. (a) Refocusing field. (b) Corresponding spatial spectrum. (c) Refocusing field. (d) Corresponding spatial spectrum.

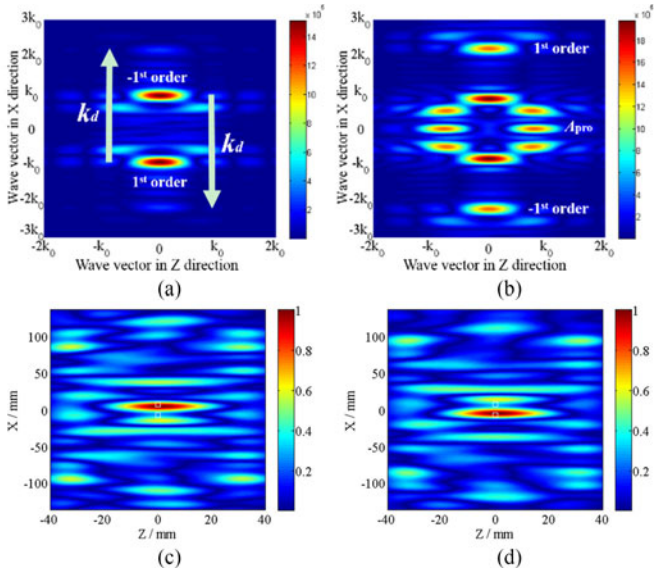

Fig. 7. Imaging results of two subwavelength separated metal spheres. (a) Operation schematic of the demodulation. (b) Combined spatial spectrum distribution of Target 1 after demodulation. (c) Corresponding inverse Fourier transform result of (b), which is the image of Target 1. The small bricks stand for the exact positions of the targets. Similarly, the image of Target 2 can be had, as shown in (d).

ably compared with the images shown in Fig. 7(c) and (d), especially along the *z*-direction. Finally, combining the images of the two targets together, we can get the image result with both targets, as shown in Fig. 8(c). To get a clear view of the resolution, the cross-section profile of the image along the red dotted line in Fig. 8(c) is shown in Fig. 8(d). The two targets separated by 5 mm (1/10 wavelength @ 6 GHz) can be well resolved.

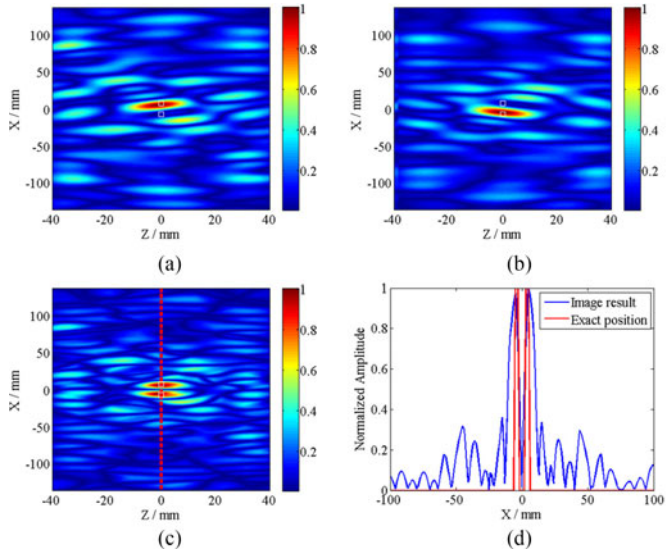

Fig. 8. Images of the two targets with informations in 0, 45, and 90 degrees combined by rotating the grating plate. (a) Image of Target 1. (b) Image of Target 2. (c) Combined imaging result of the targets. (d) Cross-section image profile along the red dotted line shown in (c).

4. Conclusion

In conclusion, the optical far-field super-lens is introduced to microwave imaging application, accompanied by the corresponding image reconstruction method based on TR technology. It has been proved that in the far-field, both the propagative and evanescent informations can be recorded. With TR technique, the near-field scattered fields can be reconstructed. Imaging results show that the system can present an imaging resolution of 5 mm, which is one tenth of the central wavelength. Meanwhile, the imaging system can provide much clearer 2-D images of the targets by combining the informations of the targets in several directions through rotating the grating plate. This kind of method provides a totally new alternative method for far-field super-resolution imaging.

References

[1] J. B. Pendry, "Negative refraction makes a perfect lens," *Phys. Rev. Lett.*, vol. 85, no. 18, pp. 3966–3969, Oct. 2000.
[2] N. Fang, H. Lee, and C. Sun, "Sub-diffraction-limited optical imaging with a silver superlens," *Science*, vol. 308, no. 5721, pp. 534–537, Apr. 2005.
[3] S. Durant, Z. Liu, J. M. Steele, and X. Zhang, "Theory of the transmission properties of an optical far-field superlens for imaging beyond the diffraction limit," *J. Opt. Soc. Amer. B*, vol. 23, no. 11, pp. 2383–2392, Nov. 2006.
[4] Z. Liu *et al.*, "Far-field optical superlens," *Nano Lett.*, vol. 7, no. 2, pp. 403–408, Jan. 2007.
[5] Y. Xiong, Z. Liu, C. Sun, and X. Zhang, "Two-dimensional imaging by far-field superlens at visible wavelengths," *Nano Lett.*, vol. 7, no. 11, pp. 3360–3365, Oct. 2007.
[6] W. Zhang, H. Chen, and H. O. Moser, "Subwavelength imaging in a cylindrical hyperlens based on S-string resonators," *Appl. Phys. Lett.*, vol. 98, no. 7, pp. 073501-1–073501-3, Feb. 2011.
[7] B. Zheng *et al.*, "Broadband subwavelength imaging using non-resonant metamaterials," *Appl. Phys. Lett.*, vol. 104, no. 7, pp. 073502-1–073502-4, Feb. 2014.
[8] G. Lerosey, J. de Rosny, A. Tourin, and M. Fink, "Focusing beyond the diffraction limit with far-field time reversal," *Science*, vol. 315, no. 5815, pp. 1120–1122, Feb. 2007.
[9] P. Kosmas and C. M. Rappaport, "Time reversal with the FDTD method for microwave breast cancer detection," *IEEE Trans. Microw. Theory Techn.*, vol. 53, no. 7, pp. 2317–2323, Jul. 2005.
[10] J. A. Encinar, "Mode-matching and point-matching techniques applied to the analysis of metal-strip-loaded dielectric antennas," *IEEE Trans. Antennas Propag.*, vol. 38, no. 9, pp. 1405–1412, Sep. 1990.
[11] R. Petit, *Electromagnetic Theory of Gratings*, New York, NY, USA: Springer-Verlag, 1980.